7th International Conference on Multiphase Flow,
ICMF 2010, Tampa, FL, May 30 – June 4, 2010

Shock Theory of a Bubbly Liquid in a Deformable Tube

K. Ando*, T. Sanada†, K. Inaba‡,

J. E. Shepherd*, T. Colonius* and C. E. Brennen*

* Department of Mechanical Engineering, California Institute of Technology, Pasadena, CA 91125, USA

† Department of Mechanical Engineering, Shizuoka University, Hamamatsu 432-8561, Japan

† Department of Mechanical Engineering and Science, Tokyo Institute of Technology, Tokyo 152-8550, Japan

kando@caltech.edu, ttsanad@ipc.shizuoka.ac.jp, inaba@mech.titech.ac.jp

joseph.e.shepherd@caltech.edu, colonius@caltech.edu and brennen@caltech.edu

Keywords: Fluid-structure interaction, bubbly water hammer

Abstract

Shock propagation through a bubbly liquid filled in a deformable cylindrical tube is considered. Quasi-one-dimensional bubbly flow equations that include fluid-structure interaction are formulated, and the steady shock relations are derived. Experiments are conducted in which a free-falling steel projectile impacts the top of an air/water mixture in a polycarbonate tube, and stress waves in the tube material are measured. The experimental data indicate that the linear theory cannot properly predict the propagation speeds of shock waves in mixture-filled tubes; the shock theory is found to more accurately estimate the measured wave speeds.

Introduction

A fundamental understanding of fluid-structure interaction (FSI) is of great importance in industrial piping systems, underwater explosions and turbomachinary (Wylie and Streeter 1993; Cole 1948; Brennen 1994). These flows often involve gas (or vapor) bubbles that alter the dynamics of the fluid dramatically (Brennen 1995, 2005). Dynamic loading of fluid-filled, deformable tubes has been extensively studied as an FSI model problem (Tijsseling 1996; Ghidaoui et al. 2005). Liquid-filled tubes were first studied by Korteweg (1878) and Joukowsky (1898), who introduced a linear wave speed that accounts for the compressibility of both the liquid and the structure. The Korteweg–Joukowsky wave speed in the case of bubbly liquids was later validated by Kobori et al. (1955). However, to the authors' knowledge, a (nonlinear) shock theory that includes both structural compressibility and bubbles has not been presented previously.

The goal of this paper is thus to develop the steady shock theory for a bubbly liquid in a deformable cylindrical tube. We describe the bubbly flow model and formulate quasi-one-dimensional equations for cylindrical tubes, and derive the steady shock relations. Also, we report on experiments in which a free-falling steel projectile impacts the top of a polycarbonate tube filled with air/water mixtures with void fractions up to one percent. Stress waves in the tube material are measured and used to infer wave speeds. The measured wave speeds are compared to the shock theory, and the model limitations are discussed.

Nomenclature

Roman symbols

a	Internal tube radius (m)
A	Internal tube area (m^2)
B	Tensile strength of a liquid (Pa)
c	Sonic speed ($m\,s^{-1}$)
c_J	Korteweg–Joukowsky wave speed ($m\,s^{-1}$)
E	Young's modulus (Pa)
h	Tube wall thickness (m)
K	Bulk modulus (Pa)
M_s	Shock Mach number ($-$)
n	Bubble number density (m^{-3})
p	Pressure (Pa)
R	Bubble radius (m)
t	Time (s)
u	Velocity ($m\,s^{-1}$)

U_s Shock speed ($\mathrm{m\,s^{-1}}$)
x Spatial coordinate (m)

Greek symbols
α Void fraction ($-$)
γ Stiffness of a liquid ($-$)
ϵ_θ Hoop strain ($-$)
κ Polytropic index ($-$)
ξ Fluid-structure interaction parameter ($-$)
ρ Density ($\mathrm{kg\,m^{-3}}$)
Υ Surface tension ($\mathrm{N\,m^{-1}}$)

Subscripts
g Gas property
H Quantity (far) behind a shock
l Liquid property
s Solid property
0 Initial (undisturbed) value

FSI bubbly flow model

Mixture-averaged equations. The liquid and disperse phases are treated as a continuum in order to evaluate the average mixture dynamics. We first review the bubbly flow model (Ando 2010) based on the ensemble-averaging technique of Zhang and Prosperetti (1994). The continuum model assumes that (a) fission and coalescence of the (spherical) bubbles do not occur; (b) direct interactions between the bubbles are negligible; (c) wavelengths in the mixture are large compared to the average inter-bubble distance; (d) the bubbles advect with the ambient liquid velocity; and (e) density and velocity fluctuations in the liquid phase due to the bubble oscillations are uncorrelated. The assumptions (b) to (d) are generally valid in the dilute limit. The model limitations are further discussed in Ando (2010).

With these assumptions, we write the one-dimensional mixture conservation equations with no FSI as

$$\frac{\partial \rho}{\partial t} + \frac{\partial \rho u}{\partial x} = 0, \tag{1}$$

$$\frac{\partial \rho u}{\partial t} + \frac{\partial}{\partial x}\left(\rho u^2 + p_l\right) = \frac{\partial \tilde{p}}{\partial x}, \tag{2}$$

$$\frac{\partial n}{\partial t} + \frac{\partial n u}{\partial x} = 0, \tag{3}$$

where ρ is the mixture density, u is the mixture velocity, p_l is the averaged liquid pressure, and n is the number of bubbles per unit volume of the mixture. For dilute mixtures, the mixture density is well approximated by $(1-\alpha)\rho_l$ where ρ_l is the liquid density and the α is the void fraction defined as

$$\alpha = \frac{4\pi}{3} n \int_0^\infty R^3 f(R_0) dR_0. \tag{4}$$

Here, R is the bubble radius, R_0 is the equilibrium bubble radius corresponding to the ambient pressure ($p_{l0} = 101$ kPa), and $f(R_0)$ represents the normalized bubble size distribution. Assuming that the liquid-phase flow is homentropic, the averaged liquid pressure will be described by the Tait equation of state (Thompson 1972),

$$\frac{p_l + B}{p_{l0} + B} = \frac{1}{\rho_{l0}^\gamma}\left(\frac{\rho}{1-\alpha}\right)^\gamma, \tag{5}$$

where ρ_{l0} is the reference liquid density at p_{l0}, and γ and B denote the stiffness and tensile strength of the liquid, respectively. For water, we take $\gamma = 7.15$ and $B = 304$ MPa. The term $\tilde{p}$ in equation (2) represents pressure fluctuations due to the phase interactions and vanishes in the equilibrium state. If one neglects the phase interaction term, the ensemble-averaged mixture equations are essentially the same as the volume-averaged equations of van Wijngaarden (1972).

Quasi-one-dimensional FSI equations. In what follows, we include the effect of FSI in the mixture-averaged equations (1) to (3). Let A be the internal cross-sectional area of the cylindrical tube. We now make the following simplifications: (f) the tube area changes are small and gradual in the flow direction; (g) the tube inertia is negligible; (h) the liquid pressure is only balanced by the hoop stress; and (i) the viscous shear stress on the inner wall is negligible. As a result of these assumptions, the tube area is given quasistatically by (Tijsseling 1996)

$$A = A_0\left[1 + \frac{2a_0}{Eh}(p_l - p_{l0})\right], \tag{6}$$

where a is the internal tube radius, h is the wall thickness, E is Young's modulus of the tube material, and the subscript 0 denotes the initial (undisturbed) values.

With a conventional control volume analysis, the quasi-one-dimensional versions of equations (1) to (3) become

$$\frac{\partial \rho A}{\partial t} + \frac{\partial \rho u A}{\partial x} = 0, \tag{7}$$

$$\frac{\partial \rho u A}{\partial t} + \frac{\partial}{\partial x}\left(\rho u^2 A + p_l A - \frac{A_0 a_0}{Eh} p_l^2\right) = \frac{\partial \tilde{p} A}{\partial x}, \tag{8}$$

$$\frac{\partial n A}{\partial t} + \frac{\partial n u A}{\partial x} = 0. \tag{9}$$

Steady shock speeds

Sonic speeds. We first derive the sonic speeds of the bubbly liquid with and without FSI. For convenience, we define the bulk modulus of the mixture, K, as

$$\frac{1}{K} = \frac{1-\alpha}{K_l} + \frac{\alpha}{K_g}, \tag{10}$$

where K_l and K_g are the bulk moduli of the liquid and gas, respectively. For Tait liquids, we have $K_l = \gamma(p_l + B)$. If the effects of the vapor and the surface tension are neglected, we may take $K_g = \kappa p_l$ where κ is the polytropic index of the gas. With the mixture bulk modulus (10), the sonic speed of the mixture (in which the bubbles behave quasistatically) becomes

$$c = \sqrt{\frac{K}{\rho}} = \sqrt{\frac{K_l/\rho}{1 + \alpha\left(\frac{K_l}{K_g} - 1\right)}}. \tag{11}$$

In the dilute limit ($\alpha \to 0$),

$$c \to c_l = \sqrt{\frac{K_l}{\rho_l}}, \tag{12}$$

where c_l is the sonic speed of the liquid alone.

We now include the effect of the structural compressibility on the mixture sonic speed (11). The Korteweg–Joukowsky wave speed for the mixture is evaluated as

$$c_J = \frac{c}{\sqrt{1+\xi}} = \sqrt{\frac{K_l/\rho}{1 + \alpha\left(\frac{K_l}{K_g} - 1\right) + \xi_l}}, \tag{13}$$

where ξ and ξ_l determine the extent of fluid-structure coupling for the cases of the mixture and the liquid alone, respectively:

$$\xi = \frac{2Ka_0}{Eh}, \quad \xi_l = \frac{2K_l a_0}{Eh}.$$

Note that the structural compressibility reduces the linear wave speed in the mixture (i.e. $c_J < c$). In the dilute limit,

$$c_J \to c_{lJ} = \frac{c_l}{\sqrt{1+\xi_l}}, \tag{14}$$

where c_{lJ} is the (non-dispersive) wave speed for the case of the liquid alone.

Steady shock relations. We develop the steady shock relations for a shock in a bubbly liquid in a deformable cylindrical tube. In front of the shock, the bubbles are in equilibrium at (R_0, T_0, p_{l0}) where T_0 is the initial temperature of the bubble contents. Far downstream of the shock front, the bubble dynamics are finally damped out and the bubbles are once again in equilibrium at (R_H, T_0, p_{lH}) where R_H is the new equilibrium radius corresponding to shock pressure $p_{lH} > p_{l0}$. The quasi-one-dimensional equations (7) to (9) are now written in a coordinate system ($x' = x - U_s t$) moving with the shock velocity U_s:

$$\frac{\partial}{\partial x'}(\rho u' A) = 0, \tag{15}$$

$$\frac{\partial}{\partial x'}\left(\rho u'^2 A + g(p_l) - \tilde{p}A\right) = 0, \tag{16}$$

$$\frac{\partial}{\partial x'}(n u' A) = 0, \tag{17}$$

where

$$g(p_l) = A_0\left(1 - \frac{2p_{l0}a_0}{Eh}\right)p_l + \frac{A_0 a_0}{Eh}p_l^2. \tag{18}$$

Integrating equations (15) to (17) from upstream (denoted by subscript 0) to far downstream (denoted by subscript H), it transpires that, independent of the detailed shock structure,

$$-\rho_H u'_H A_H = \rho_0 U_s A_0, \tag{19}$$

$$\rho_H u'^2_H A_H + g(p_{lH}) = \rho_0 U_s^2 A_0 + g(p_{l0}), \tag{20}$$

$$-n_H u'_H A_H = n_0 U_s A_0, \tag{21}$$

where $\rho_0 = (1-\alpha_0)\rho_{l0}$ and $\rho_H = (1-\alpha_H)\rho_{lH}$.

The shock pressure, p_{lH}, may be written as

$$p_{lH} = \left(p_{l0} - p_v + \frac{2\Upsilon}{R_0}\right)\left(\frac{R_H}{R_0}\right)^{-3\kappa} + p_v - \frac{2\Upsilon}{R_H}, \tag{22}$$

where κ is set to unity because the bubble temperature finally returns to T_0. If vapor pressure p_v and surface tension Υ are neglected, equation (22) reduces to

$$p_{lH} = p_{l0}\left(\frac{R_H}{R_0}\right)^{-3}. \tag{23}$$

It follows from equations (19) and (21) that

$$n_H = n_0\left[(1-\alpha_0)\left(\frac{p_{l0}+B}{p_{lH}+B}\right)^{\frac{1}{\gamma}} + \frac{4\pi}{3}n_0\int_0^\infty R_H^3 f(R_0)dR_0\right]^{-1}. \tag{24}$$

With the aid of equations (22) and (24), the void fraction α_H corresponding to p_{lH} is computed by equation (4). With the neglect of vapor pressure and surface tension, equation (24) reduces to

$$n_H = n_0\left[(1-\alpha_0)\left(\frac{p_{l0}+B}{p_{lH}+B}\right)^{\frac{1}{\gamma}} + \alpha_0\frac{p_{l0}}{p_{lH}}\right]^{-1}, \tag{25}$$

and the void fraction at p_{lH} is

$$\alpha_H = \frac{4\pi}{3}n_H\int_0^\infty R_H^3 f(R_0)dR_0 = \left[1 + \frac{1-\alpha_0}{\alpha_0}\frac{p_{lH}}{p_{l0}}\left(\frac{p_{l0}+B}{p_{lH}+B}\right)^{\frac{1}{\gamma}}\right]^{-1}. \tag{26}$$

From equations (19) and (20), the steady shock speed becomes

$$U_s = \sqrt{\frac{g(p_{lH}) - g(p_{l0})}{\rho_0 A_0\left(1 - \frac{\rho_0 A_0}{\rho_H A_H}\right)}}, \tag{27}$$

and the induced velocity far downstream of the shock front is then given by

$$u_H = u'_H + U_s = \left(1 - \frac{\rho_0 A_0}{\rho_H A_H}\right) U_s. \qquad (28)$$

It is readily shown that the shock speed (27) approaches the Joukowsky wave speed (13) if the shock strength is infinitesimal. Consequently, the shock Mach number may be defined as

$$M_s = \frac{U_s}{c_J}. \qquad (29)$$

Gas-phase nonlinearity. We document the steady shock relations for the case of bubbly water with $\xi_l = 6.14$ where the value of ξ_l is computed based on the properties of the polycarbonate tube that is used in the experiments. For simplicity, we ignore the effects of vapor pressure and surface tension. Figure 1 demonstrates the effects of the initial void fraction and the shock pressure on the shock speed and Mach number. Note that $p_{lH} = p_{l0}$ indicates the linear wave cases, in which the shock speeds reduce to the sonic speeds. It follows from figure 1 (top) that the reduction in the shock speed due to structural compressibility is minimized for finite values of α_0 since the gas-phase compressibility dominates over the compressibility of the water and structure. It is also seen that the shock speeds are greatly reduced by even a tiny void fraction. Moreover, unless the void fraction is extremely small, the finite shock strength yields a significant deviation from the linear wave speed due to the nonlinearity associated with the gas-phase compressibility. As a result, the shock Mach number increases as the void fraction increases as seen in figure 1 (bottom). We note that the shock Mach numbers are only slightly greater than 1 for the case of water alone ($\alpha_0 = 0$) since the pressure perturbations up to several hundred atmospheres remain very weak (Thompson 1972).

To quantify the effect of the gas-phase nonlinearity, we further examine the steady shock relations. For the case of infinitesimal shock strength ($\Delta p_l = p_{lH} - p_{l0} \ll p_{l0}$), the shock speed (27) can be approximated by

$$U_s \approx c_J \left(1 + \frac{\Delta p_l}{\hat{K}}\right), \qquad (30)$$

where $\hat{K}$ is defined as

$$\hat{K} = c_J \left(\frac{dU_s}{d\Delta p_l}\bigg|_{\Delta p_l = 0+}\right)^{-1}. \qquad (31)$$

In the limits of $\alpha_0 \to 0$ and $\xi \to 0$, we find $\hat{K} \to 4K_l/(\gamma + 1)$; $\hat{K}$ may thus be called the *modified* bulk modulus. It follows from equation (30) that the linear

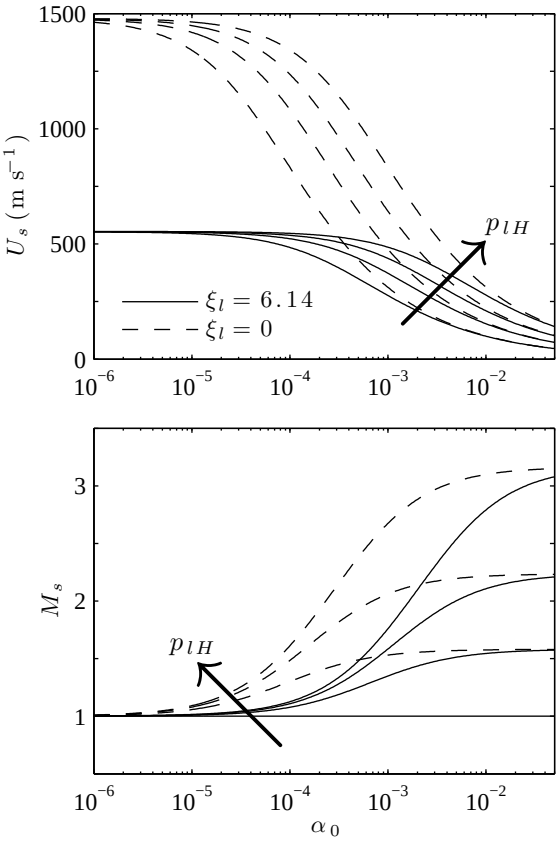

Figure 1: Steady shock speeds (top) and shock Mach numbers (bottom) in bubbly water. The curves are parameterized by $p_{lH}/p_{l0} = 1, 2.5, 5, 10$.

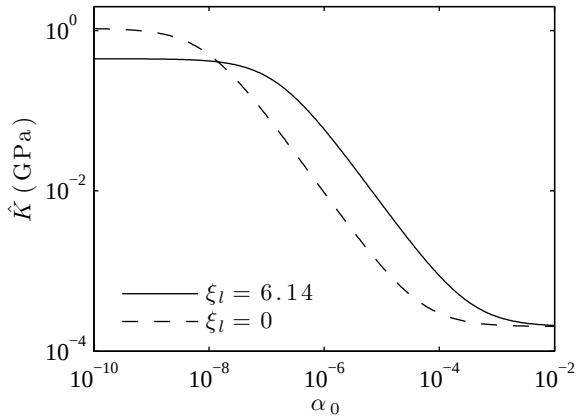

Figure 2: Modified bulk modulus of bubbly water.

theory (where the relation $U_s = c_J$ holds) is effectively valid under the condition $\hat{K} \gg \Delta p_l$. Hence, the modified bulk modulus, $\hat{K}$, of the mixture can be regarded as a measure of the nonlinearity in the sense that larger values of $\hat{K}$ make the linear theory applicable to a broader range of the shock pressures. The modified bulk moduli of bubbly water are plotted as a function of α_0 in figure 2. It turns out that even a small void fraction yields a several-orders-of-magnitude reduction in the value of $\hat{K}$. This implies that the applicability of the linear theory is limited in the case of bubbly mixtures.

Waterhammer experiments

Experimental setup. Experiments were conducted in order to examine the steady shock theory. The experimental apparatus depicted in figure 3 is similar to that of Inaba and Shepherd (2010), and consists of a vertical polycarbonate tube (PCT0021.25, San Diego Plastics; $E = 2.13$ GPa, $\rho_s = 1200\ \mathrm{kg\,m^{-3}}$, $a_0 = 3h = 19.1$ mm) filled with an air/water mixture. A barrel is mounted above the tube and a 1.50-kg cylindrical steel projectile falls under gravity, g. The free-falling projectile (with drop height $H_p = 2$ m or 0.5 m) impacts a 0.42-kg polycarbonate buffer inserted into the top of the tube rather than directly hitting the bubbly liquid surface. Stress waves in the tube are measured using six strain gauges (SR-4, Vishay; denoted by g1 to g6 in figure 3) placed at intervals of 100 mm along the tube and oriented in the hoop direction; the signals are processed using a signal conditioning amplifier (2300 System, Vishay), and are stored in a digital recorder (NI 6133, National Instruments; sampling rate 2.5 MHz).

Method of bubble generation. The bubbles are created using a bubble generator consisting of an aluminum plate and capillary tubes (TSP020150, Polymicro Technologies; inner diameter 20 μm); the intent is to create small bubbles and as homogeneous a mixture as possible. Up to an initial void fraction of $\alpha_0 = 0.0056$, 91 capillary tubes are used; for higher void fractions, the number increases to 217. The capillary tubes are located in the drilled holes of the plate and are fastened with epoxy. One side of the plate is tightly covered with a chamber. The chamber is pressurized, and the air is injected, due to the pressure head, into the fluid column. The injected bubbles rise upward to the column surface, and eventually escape from an air outlet in the buffer.

Distilled water is used for the case of no air injection; otherwise, tap water is used. Note that the number of tiny bubbles present in tap water is negligible compared to that of the injected air. The water temperature is kept $23\,^{\circ}$C so that the vapor pressure is much smaller than

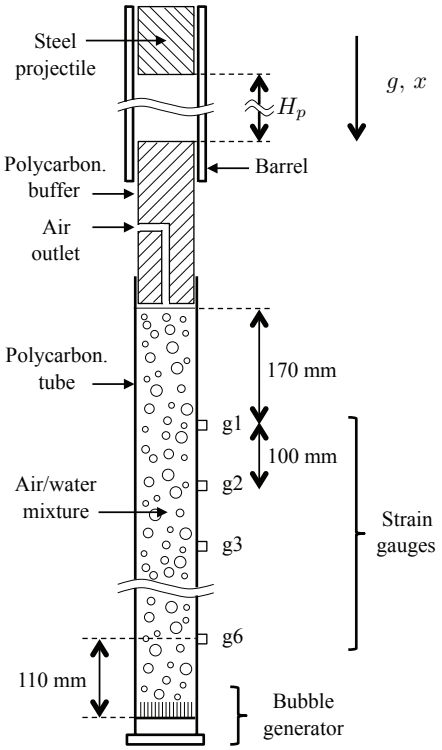

Figure 3: Schematic of the experimental setup.

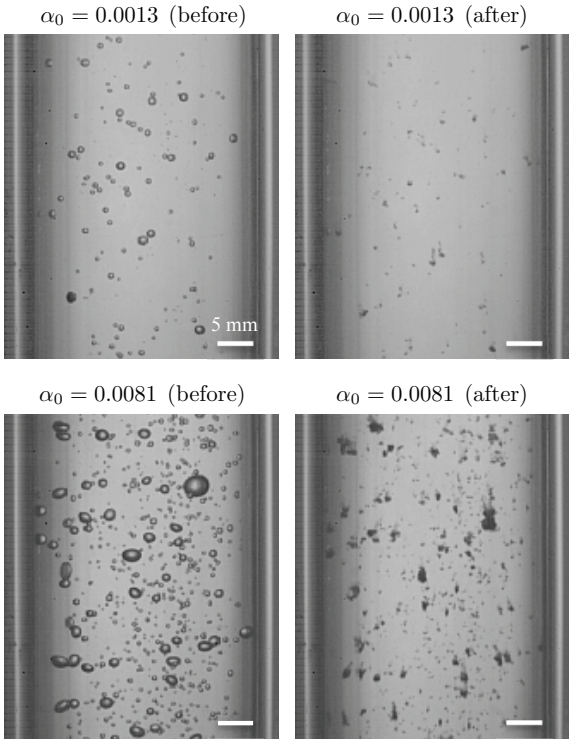

Figure 4: Images of the injected bubbles before and after the primary wave passage.

one atmosphere.

Images of the bubbles are captured by a high-speed video camera (Phantom v7.3, Vision Research) with recording rate 20000 frames per second. A white LED lamp (Model 900445, Visual Instrumentation Corporation) is used for backlighting. A water jacket is attached outside the tube to minimize image distortion. Images of the initial bubbles and the collapsing bubbles due to the shock loading with $H_p = 2$ m are shown in figure 4. The initial bubble size is found to be broadly distributed (i.e. the mixture is polydisperse), and the mixture is nearly homogeneous. Moreover, for the higher void fraction case, we observe fission of the larger bubbles. Possible mechanisms for the fission are a re-entrant jet and a Rayleigh-Taylor-type instability (Brennen 2002; Johnsen and Colonius 2009).

The initial void fraction (up to one percent) is estimated based on the difference in the column height with and without the air injection. Uncertainty in this measurement is ± 0.1 mm except for the case of the highest void fraction, $\alpha_0 = 0.01$, in which the column surface waves increase the uncertainty to ± 0.5 mm. In the waterhammer experiments, the following void fractions were tested: $\alpha_0 = 0$ (no air injection), 0.0013 ± 0.0001, $0.0024 \pm 0.0001, 0.0056 \pm 0.0001, 0.0081 \pm 0.0001$ and 0.010 ± 0.001.

Buffer dynamics. In the present experiments, the liquid pressure is unknown. Hence, the buffer velocity $\dot{x}_b$ (or the piston velocity u_H in the shock theory) is critical to estimate to validate the shock theory. Three experimental runs were conducted for each case of H_p and α_0. For every run, the buffer position x_b was recorded using the high-speed camera with recording rate of 32000 frames per second, and the position history was extracted from the movies with MATLAB image processing.

The buffer dynamics may be described by Newton's second law (Dashpande et al. 2006; Shepherd and Inaba 2009). For simplicity, the buffer is treated as a rigid body and wall friction is neglected. The equation of motion of the buffer is then given by

$$M_b \ddot{x}_b = -\Delta p_l A_0, \tag{32}$$

where M_b is the mass of the buffer and the right-hand side represents the pressure force acting on the bottom of the buffer. In the linear case, this pressure force may be approximated by $\Delta p_l A_0 = \rho_0 c_J \dot{x}_b A_0$ as can be derived from equations (19) and (20). Integrating equation (32) once, we get a solution of the form,

$$\dot{x}_b = \dot{x}_{b0} \exp\left(-\frac{t}{\tau}\right), \tag{33}$$

where $\dot{x}_{b0}$ is the initial buffer velocity and τ is the relaxation time for the exponential decay:

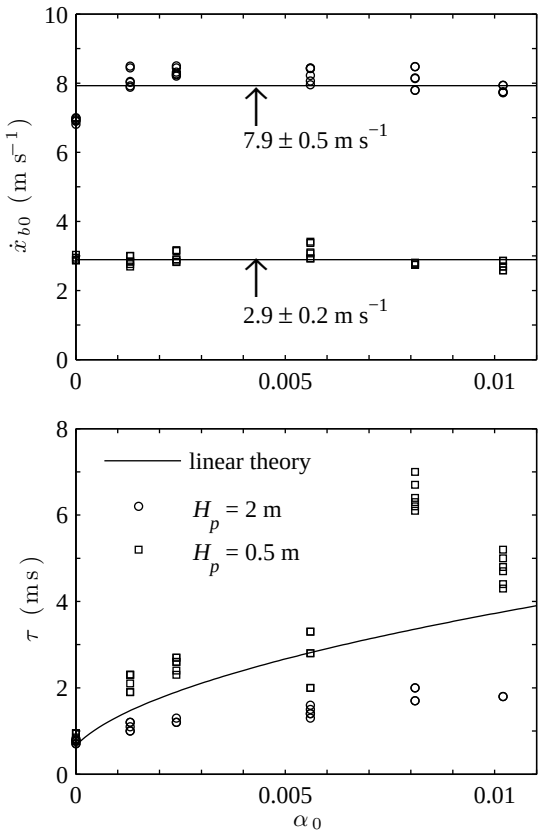

Figure 5: The initial buffer velocity (top) and the relaxation time (bottom).

$$\tau = \frac{M_b}{\rho_0 c_J A_0}. \tag{34}$$

Thus, the evolution of the buffer position is expressed by an exponential function.

The measured buffer positions were fitted to an exponential by the least-squares method. The resulting buffer velocity $\dot{x}_{b0}$ and relaxation time τ are presented in figure 5. We find that the buffer velocity $\dot{x}_{b0}$ is only weakly dependent on the void fraction and therefore seems to depend only on the drop height H_p; it is 7.9 ± 0.5 m s^{-1} and 2.9 ± 0.2 m s^{-1} for $H_p = 2$ m and 0.5 m, respectively, where the error bounds represent the standard deviation of all the runs. It follows from figure 5 (bottom) that the linear theory (34) is in qualitative agreement with the experimental data and is particularly good for the case of no air injection. Moreover, the relaxation time decreases as the initial buffer velocity increases. Since a stronger shock leads to a more violent bubble collapse, the buffer momentum may decay more rapidly due to bubble-dynamic energy dissipation. Note that if

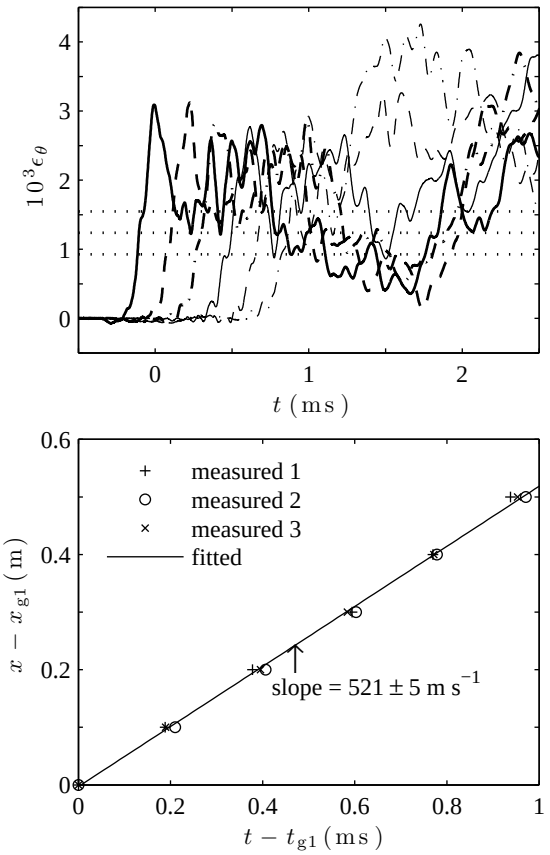

Figure 6: Evolution of hoop strains (top) and the locations of the primary wave fronts (bottom) for $H_p = 2$ m and $\alpha_0 = 0$. The dotted lines (top) denote the threshold values used to determine the wave fronts.

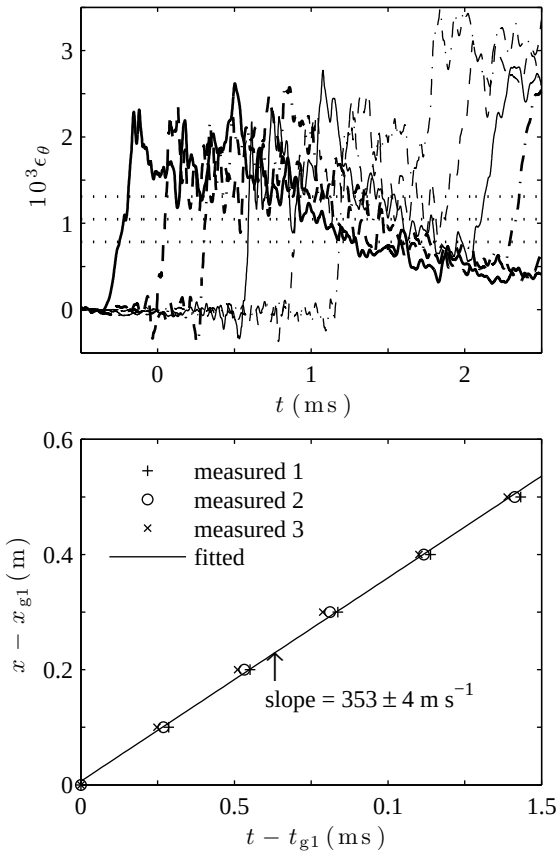

Figure 7: As figure 6, but with $H_p = 2$ m and $\alpha_0 = 0.0081$.

the relaxation time is longer than the time required for the shock to reach the last strain gauge (g6), the piston velocity will not change within the measurement period.

Primary wave speeds. We examine the shock (or primary) waves in the experiments that are characterized by the drop height H_p and the initial void fraction α_0. To confirm repeatability in the measurements, three experimental runs were conducted for each case of H_p and α_0. In what follows, we choose some particular cases, and investigate the wave structures and the wave speeds.

The evolution of the hoop strains for the case of $H_p = 2$ m and $\alpha_0 = 0$ is shown in figure 6 (top). Every strain gauge records the primary wave following a small-amplitude precursor that propagates essentially with the sonic speed of the tube material (Skalak 1956). It also records a wave reflected from the tube bottom, and significant wave dispersion. Moreover, the primary wave noticeably decays within the measurement period; thus the decay time is comparable to the relaxation time of the piston velocity computed in figure 5. Consequently, the unsteadiness of the buffer dynamics cannot be ignored.

In figure 6 (bottom), the primary wave speeds are computed. For comparative purposes, three threshold strain values (30, 40 and 50 percent of the maximum strain measured at the strain gauge g1 before the reflected wave is observed) are used to determine the positions of the wave fronts. Then, the wave speed was obtained from the slope of a linear least-squares fit to the wave front positions; the standard deviation of the slope was also computed. The computed speed ($521\ \mathrm{m\,s^{-1}}$) is in reasonable agreement with the Korteweg–Joukowsky wave speed ($c_{lJ} = 553\ \mathrm{m\,s^{-1}}$), and the the dispersion due to the thresholding is very small. This suggests that the linear theory is effectively valid for the case of pure water, even though the wave is dispersive and unsteady.

The bubbly water case ($H_p = 2$ m, $\alpha_0 = 0.0081$) is presented in figure 7. Now that the bubble dynamics play a role, the structural response manifests more complex structures than in the pure liquid case. The comparison of the figures 6 and 7 (top) reveals that the bubbles reduce the tube deformation. This is due to the fact that

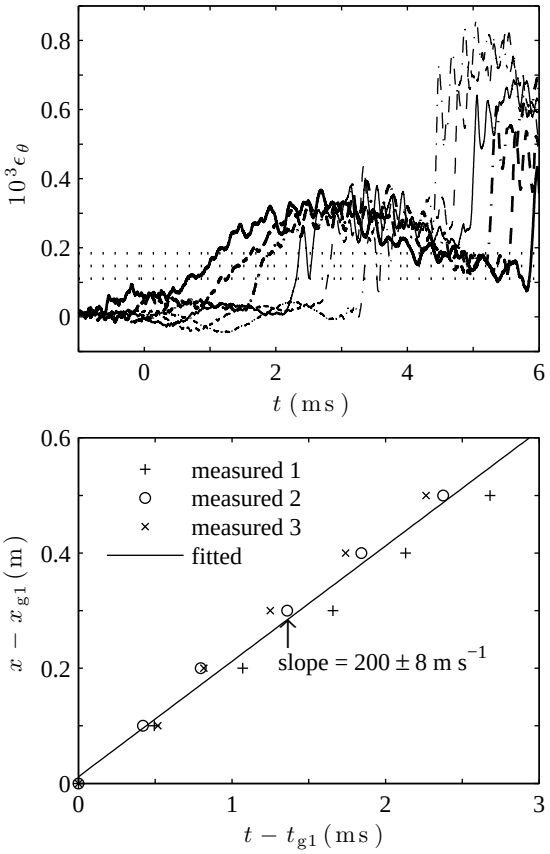

Figure 8: As figure 6, but with $H_p = 0.5$ m and $\alpha_0 = 0.0081$.

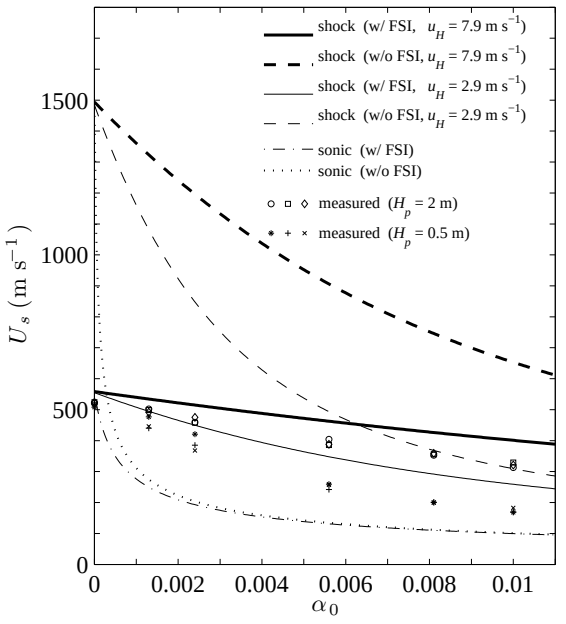

Figure 9: Comparison of the theoretical and measured wave speeds.

some fraction of the potential energy of the projectile is absorbed as bubble-dynamic work. Moreover, the wave speed is reduced by the bubbles. To further see the effect of the bubbles, the case of the lower drop height ($H_p = 0.5$ m, $\alpha_0 = 0.0081$) is presented in figure 8. In this case, the wave propagation is evidently unsteady. The unsteadiness may also result from the fact that the relaxation time for the piston velocity and the measurement time are comparable. As a result of the unsteadiness, the threshold value becomes more critical, and the standard deviation in the computed wave speed becomes larger. We should note that the lower piston velocity reduces the wave speed. This is the effect of the gas-phase nonlinearity as pointed out in figure 4.

We now compare the steady shock theory to the experimental data. Despite the unsteady buffer dynamics, we use the initial buffer velocity $\dot{x}_{b0} = 7.9\ \mathrm{m\,s^{-1}}$ (or $2.9\ \mathrm{m\,s^{-1}}$) for $H_p = 2$ m (or 0.5 m) to complete the steady shock relations. Since vapor pressure at the room temperature is negligible compared to the atmospheric pressure and surface tension may not be very important for the bubble sizes in the experiments, we neglect the vapor pressure and the surface tension (i.e. $p_v = 0$, $\Upsilon = 0$) in computing the shock relations. Figure 9 compares the measured wave speeds to the theory including both the sonic and shock speeds. The error bars are small (as seen in figures 6 to 8) and omitted for clarity. The measured speeds for the cases with air injection clearly show differences from the sonic speeds, and those for $H_p = 2$ m are larger than those for $H_p = 0.5$ m. These indicate the effect of the gas-phase nonlinearity on the wave speeds. The shock theory with FSI is found to more accurately capture the trend with increasing α_0 than the shock theory without FSI and the linear theory. It is therefore concluded that both FSI and the nonlinear effect need to be considered to accurately estimate the propagation speeds of finite-amplitude waves in mixture-filled pipes. However, the agreement between the present theory and the experiments is qualitative rather than quantitative. The model limitations are discussed below to try to account for the discrepancy between the present theory and the experiments.

Model limitations. One of the most obvious limitations in the theory is related to the assumption of steady wave propagation. The strain evolution in figures 6 to 8 (top) demonstrates unsteady wave propagation in the sense that the piston velocity decays during the measurement period. Hence, the unsteadiness will deteriorate the model validity. If one quantifies the decay rate in the relaxation process, both the structural and the bubble-dynamic damping need to be included in the thoery. The viscoelasticity of the polycarbonate may affect the wave speed and damping (Meißner and Frank 1977; Gally

et al. 1979; Suo and Wylie 1990; Covas et al. 2004). The unsteady wall friction may also have some impact on the relaxation (Bergant 2001). If bubble fission occurs after passage of the shock, the fission damping needs to be included in spherical-bubble-dynamic modeling (Brennen 2002). Moreover, because polydispersity results in different frequency responses for different-sized bubbles, phase cancellations cause an apparent damping of the wave propagation (Smereka 2002; Colonius et al. 2008; Ando et al. 2009; Ando 2010).

Other limitations are the neglect of the tube inertia and the quasi-one-dimensional assumption. Since the waves are dispersive (due to the tube inertia) and of finite wave length, the wave speed as a function of the wave length cannot be accurately predicted by the current model. To quantify the effect of the tube inertia, a four-equation model describing both the fluid and the tube dynamics could be calculated (Skalak 1956; Tijsseling 1996).

Conclusions

A quasi-one-dimensional conservation law governing dilute bubbly flows in a deformable cylindrical tube is formulated, and the steady shock relations are derived. The modified bulk modulus of the mixture is introduced, and the nonlinear effect due to the gas-phase compressibility is shown to be important for shock propagation. The present FSI shock theory is found to be in better agreement with the measured wave speeds than the linear theory or the shock theory without FSI. This suggests that both FSI and the gas-phase nonlinearity need to be included to accurately predict the propagation speeds of finite-amplitude waves in mixture-filled pipes.

Acknowledgements

The authors would like to express their thanks to T. Nishiyama for his help with the experimentation, J. S. Damazo and R. Porowski for the bubble images, and S. Hori for his observations about the experimental data. This work was supported by ONR Grant No. N00014-06-1-0730.

References

K. Ando. *Effects of polydispersity in bubbly flows*. PhD Thesis, California Institute of Technology, 2010.

K. Ando, T. Colonius, and C. E. Brennen. Improvement of acoustic theory of ultrasonic waves in dilute bubbly liquids. *J. Acoust. Soc. Am.*, 126:EL69–EL74, 2009.

A. Bergant. Developments in unsteady pipe flow friction modeling. *J. Hydraul. Res.*, 39:249–257, 2001.

C. E. Brennen. *Hydrodynamics of Pumps*. Oxford University Press, 1994.

C. E. Brennen. *Cavitation and Bubble Dynamics*. Oxford University Press, 1995.

C. E. Brennen. Fission of collapsing cavitation bubbles. *J. Fluid Mech.*, 472:153–166, 2002.

C. E. Brennen. *Fundamentals of Multiphase Flow*. Cambridge University Press, 2005.

R. H. Cole. *Underwater Explosions*. Princeton University Press, 1948.

T. Colonius, R. Hagmeijer, K. Ando, and C. E. Brennen. Statistical equilibrium of bubble oscillations in dilute bubbly flows. *Phys. Fluids*, 20:040902, 2008.

D. Covas, I. Stoianov, J. Mano, H. Romas, N. Graham, and C. Maksimovic. The dynamic effect of pipe-wall viscoelasticity in hydraulic transients (Part 1. experimental analysis and creep characterization). *J. Hydraul. Res.*, 42:516–530, 2004.

V. S. Dashpande, A. Heaver, and N. A. Fleck. An underwater shock simulator. *Proc. R. Soc. A*, 462:1021–1041, 2006.

M. Gally, M. Güney, and E. Rieutord. An investigation of pressure transients in viscoelastic pipes. *J. Fluids Eng.*, 101:495–499, 1979.

M. S. Ghidaoui, M. Zhao, D. A. Mclnnis, and D. H. Axworthy. A review of water hammer theory and practice. *Appl. Mech. Rev.*, 58:49–76, 2005.

K. Inaba and J. E. Shepherd. Flexural waves in fluid-filled tubes subject to axial impact. *J. Pressure Vessel Technol.*, 132:021302, 2010.

E. Johnsen and T. Colonius. Numerical simulations of non-spherical bubble collapse. *J. Fluid Mech.*, 629:231–262, 2009.

N. E. Joukowsky. Memoirs of the Imperial Academy Society of St. Petersburg. *Proc. Amer. Water Works Assoc.*, 24:341–424, 1898.

T. Kobori, S. Yokoyama, and H. Miyashiro. Propagation velocity of pressure wave in pipe line. *Hitachi Hyoron*, 37:33–37, 1955.

D. J. Korteweg. Ueber die Fortpflanzungsgeschwindigkeit des Shalles in elastischen Röhren. *Annalen der Physik und Chemie*, 5:525–542, 1878.

E. Meißner and P.-G. Frank. Influence of pipe material on the damping of water hammer. In *Proceedings of the Seventeenth Congress of the International Association for Hydraulic Research*, August 1977.

J. E. Shepherd and K. Inaba. Shock loading and failure of fluid-filled tubular structures. In A. Shukla, G. Ravichandran, and Y. D. S. Rajapakse, editors, *Dynamic Failure of Materials and Structures*. Springer, 2009.

R. Skalak. An extension of the theory of water hammer. *Trans. ASME*, 78:105–116, 1956.

P. Smereka. A Vlasov equation for pressure wave propagation in bubbly fluids. *J. Fluid Mech.*, 454:287–325, 2002.

L. Suo and E. B. Wylie. Complex wavespeed and hydraulic transients in viscoelastic pipes. *J. Fluids Eng.*, 112:496–500, 1990.

P. A. Thompson. *Compressible-Fluid Dynamics*. McGraw-Hill, 1972.

A. S. Tijsseling. Fluid-structure interaction in liquid-filled pipe systems: A review. *J. Fluids Struct.*, 10:109–146, 1996.

L. van Wijngaarden. One-dimensional flow of liquids containing small gas bubbles. *Ann. Rev. Fluid Mech.*, 4: 369–396, 1972.

E. B. Wylie and V. L. Streeter. *Fluid Transients in Systems*. Prentice Hall, 1993.

Z. D. Zhang and A. Prosperetti. Ensemble-averaged equations for bubbly flows. *Phys. Fluids*, 6:2956–2970, 1994.